Chemistry & Biology, Vol. 11, 203–210, February, 2004, ©2004 Elsevier Science Ltd. All rights reserved. DOI 10.1016/j.chembiol.2004.01.017

Bright Fluorescent Chemosensor Platforms for Imaging Endogenous Pools of Neuronal Zinc

Christopher J. Chang,[1] Elizabeth M. Nolan,[1] Jacek Jaworski,[2] Shawn C. Burdette,[1] Morgan Sheng,[2,3] and Stephen J. Lippard[1,*]
[1]Department of Chemistry
[2]Picower Center for Learning and Memory
[3]Howard Hughes Medical Institute
Massachusetts Institute of Technology
Cambridge, Massachusetts 02139

Summary

A series of new fluorescent Zinpyr (ZP) chemosensors based on the fluorescein platform have been prepared and evaluated for imaging neuronal Zn^{2+}. A systematic synthetic survey of electronegative substitution patterns on a homologous ZP scaffold provides a basis for tuning the fluorescence responses of "off-on" photoinduced electron transfer (PET) probes by controlling fluorophore pK_a values and attendant proton-induced interfering fluorescence of the metal-free (apo) probes at physiological pH. We further establish the value of these improved optical tools for interrogating the metalloneurochemistry of Zn^{2+}; the novel ZP3 fluorophore images endogenous stores of Zn^{2+} in live hippocampal neurons and slices, including the first fluorescence detection of Zn^{2+} in isolated dentate gyrus cultures. Our findings reveal that careful control of fluorophore pK_a can minimize proton-induced fluorescence of the apo probes and that electronegative substitution offers a general strategy for tuning PET chemosensors for cellular studies. In addition to providing improved optical tools for Zn^{2+} in the neurosciences, these results afford a rational starting point for creating superior fluorescent probes for biological applications.

Introduction

Zinc is an essential element for human growth and development [1]. The brain contains the highest cellular concentrations of this vital cofactor in the body [1, 2]. In addition to the stores of tightly bound neuronal Zn^{2+} that play structural and catalytic roles in transcription factors and enzymes [1, 3], labile pools of Zn^{2+} are present in presynaptic nerve terminals throughout the central nervous system [4]. In the hippocampus, the center of learning and memory in the brain, concentrations of ionic Zn^{2+} approach 0.3 mM in the mossy fiber terminals of dentate gyrus-CA3 synapses [4].

The homeostasis of labile Zn^{2+} in the brain has diverse physiological and pathological effects [5, 6]. Chelatable Zn^{2+} released upon synaptic activity or membrane depolarization appears to modulate neurotransmission [7, 8] and contribute to long-term potentiation [9] in the hippocampal mossy fiber synapses, whereas uncontrolled Zn^{2+} release after ischemia, seizures, or traumatic head injury induces acute neuronal death [10]. The disruption of Zn^{2+} homeostasis is also implicated in the pathology of Alzheimer's disease (AD) [11, 12] and several other neurodegenerative disorders [13]. Histochemical studies of the brains of AD patients reveal high levels of chelatable Zn^{2+} in the amyloid plaques that are characteristic of the disease [14]. Moreover, mounting evidence suggests that the early stages of AD affect the hippocampal region of the brain [15].

The emerging importance of Zn^{2+} in neurological signaling and disease and some debate about its proposed functions [6, 9, 16] has generated an intense demand for tools and tactics to map the spatial and temporal distribution of cellular Zn^{2+} at a molecular level [17–33]. In this regard, fluorescent chemosensors provide a powerful approach for investigating small organic and inorganic analytes in the biological milieu [34]. Such probes are particularly valuable for the optical detection of Zn^{2+}, a closed-shell metal ion that lacks spectroscopic properties. The most common types of fluorescent chemosensors for metal ions utilize a photoinduced electron transfer (PET) signaling mechanism [21, 35]. PET sensors consist of a fluorophore platform with an appended receptor. In the absence of analyte, electrons localized on a donor atom of the receptor participate in back electron transfer with the fluorophore excited state to quench emission. Metal ion coordination induces a change in the electronic structure of the fluorophore-receptor conjugate to alleviate PET quenching and restore fluorescence. The resulting "off-on" fluorescent chemosensors offer a convenient method for detecting metal ions and other biological analytes with high spatial and temporal fidelity.

In an effort to interrogate the complex roles of Zn^{2+} in neurobiology, we have initiated a program aimed at developing Zn^{2+}-specific PET chemosensors based on the fluorescein platform (ZP = Zinpyr) [36–40]. ZP1 (**1**) and ZP2 (**2**) (Figure 1) represent first-generation synthetic probes that detect intracellular Zn^{2+} by inducing a positive fluorescence response upon metal ion complexation. These small molecule chemosensors offer a number of attractive properties for neuroscience applications, including (1) visible excitation and emission profiles to minimize cell and tissue damage and avoid autofluorescence from native cellular species, (2) high selectivity for Zn^{2+} over biologically abundant Ca^{2+} and Mg^{2+} ions, and (3) high brightness values for their Zn^{2+}-bound forms ($\epsilon \times \phi = 7.3 \times 10^4\ M^{-1}cm^{-1}$ for ZP1, $4.9 \times 10^4\ M^{-1}cm^{-1}$ for ZP2) that are up to 50-fold greater [37] than traditional quinoline-based Zn^{2+} fluorophores [31].

Despite these advantages, the ZP dyes highlight a general challenge for applying PET chemosensors toward cellular imaging: the metal binding atoms in receptors are often susceptible to protonation under physiological conditions (neutral pH, high ionic strength) [21]. This feature can severely limit the utility of any fluorescent PET probe for biological imaging applications by producing interfering fluorescence from the protonated

*Correspondence: lippard@lippard.mit.edu

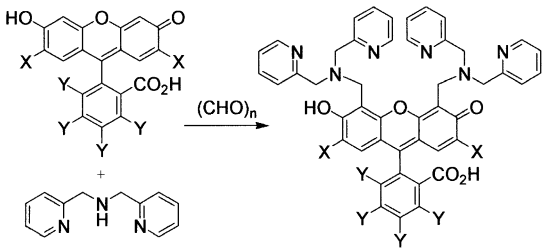

ZP1 (**1**): X = Cl, Y = H
ZP2 (**2**): X = H, Y = H
ZP3 (**3**): X = F, Y = H
ZPF1 (**4**): X = Cl, Y = F
ZPCl1 (**5**): X = Cl, Y = Cl
ZPBr1 (**6**): X = Cl, Y = Br
ZPF3 (**7**): X = F, Y = F

Figure 1. Synthesis of ZP Chemosensors

apo fluorophore at physiological pH. For example, the ZP probes exhibit relatively high pK_a values for the tertiary nitrogen atoms responsible for PET switching and, as a consequence, display accordingly high background fluorescence in their unmetalated forms (pK_a = 8.4 and ϕ = 0.38 for ZP1, pK_a = 9.4 and ϕ = 0.25 for ZP2) [37]. The magnitudes of the fluorescence responses of ZP1 and ZP2 to Zn^{2+} are greater than to protons, rendering them of considerable practical utility, but fluorescence from the protonated apo probes can hinder accurate determination of Zn^{2+} concentrations. Strategies to circumvent the obstacle of proton-induced interfering fluorescence would thus provide an important basis for the rational design of effective PET chemosensors for biological imaging and afford improved Zn^{2+}-specific probes for the neurosciences.

In this report, we present electronegative substitution as a general strategy for controlling the proton-induced interfering fluorescence of PET chemosensors. This approach is illustrated in the effective design of improved Zn^{2+}-specific probes assembled on the fluorescein platform. Specifically, we have addressed the issue of proton sensitivity by exploring the systematic effects of electronegative substitution on a homologous ZP scaffold. A palette of new chemosensor platforms bearing various halogen substitution patterns has been synthesized and evaluated for the fluorescence detection of neuronal Zn^{2+}. We find that fluorination of the fluorescein backbone results in marked reduction of proton-induced interfering fluorescence from the apo probes; the novel ZP3 (**3**) derivative offers a Zn^{2+}-specific fluorophore with notably improved brightness and dynamic range. Moreover, we demonstrate the value of these new optical tools for tracking ionic Zn^{2+} within biological samples. ZP3 has been utilized to image *endogenous* pools of Zn^{2+} in live neurons and brain slices, including fluorescence detection of ionic Zn^{2+} in isolated dentate gyrus cultures. Our results establish that electronegative substitution provides effective control of fluorophore pK_a and proton-induced interfering fluorescence under physiological conditions. This approach thus offers a general strategy and a rational basis for the design of functional PET chemosensors for biological applications.

Results and Discussion

Design and Synthesis of Electronegatively Substituted ZP Chemosensors

We reasoned that introducing electron-withdrawing substituents onto the fluorescein scaffold would reduce the pK_a values, and hence the proton sensitivity, of the tertiary nitrogen atoms responsible for PET switching. To achieve this goal, a systematic set of ZP chemosensors bearing halogen substituents appended to the top xanthenone and/or bottom aryl ring of the fluorescein backbone was prepared. The synthetic route outlined in Figure 1 [37] affords easy access of up to multigram quantities of the desired Zn^{2+} probes with no chromatographic purification.

A series of halogenated fluoresceins were isolated from acid-catalyzed fusion reactions of substituted resorcinols and phthalic anhydrides. The dyes were purified by recrystallization from ethanol/water mixtures. The preparation of fluorescein derivatives functionalized at the xanthenone 2′ and 7′ positions assures selective installation of Zn^{2+} binding groups at the 4′ and 5′ positions. Accordingly, fluorescent probes **3–7** were obtained from Mannich reactions between the appropriately derivatized fluoresceins and the iminium ion condensation product of formaldehyde and di-(2-picolyl)amine (DPA). The DPA chelators provide excellent selectivity for Zn^{2+} over biologically competing Ca^{2+} and Mg^{2+} ions [36, 37]. Pure samples of the electronegatively substituted ZP chemosensors **3–7** were obtained in good to excellent yields (80% to 95%) after filtration from the cooled reaction mixtures and subsequent recrystallization from ethanol. ZP probes **3–7** were characterized fully by ^1H, ^{13}C, and ^{19}F NMR and IR spectroscopy as well as high-resolution electrospray mass spectrometry.

Spectroscopic Properties and Optical Responses to Zn^{2+}

The electronegatively substituted ZP chemosensors **3–7** were evaluated at physiological ionic strength and pH [50 mM PIPES (piperazine-*N,N′*-bis(2-ethanesulfonic acid)), 100 mM KCl, pH 7] in the presence of EDTA (ethylenediaminetetraacetic acid) to scavenge adventitious metal ions. Spectroscopic data for the five new probes reported here and the parent compounds ZP1 and ZP2 are collected in Table 1. The optical properties of the ZP family are dominated by the xanthenone-based fluorescein chromophore. These Zn^{2+} chemosensors exhibit excitation (λ_{exc} = 490 to 534 nm) and emission (λ_{em} = 516 to 550 nm) maxima well into the visible range with Stokes shifts of approximately 20 nm. This long-wavelength regime minimizes cell and tissue damage as well as avoiding interfering autofluorescence from native cellular species. Combined with high brightness values derived from sizeable extinction coefficients (ϵ = 4.4 × 10^4 to 1.2 × 10^5 $M^{-1}cm^{-1}$) and quantum yields (ϕ = 0.36 to 0.92) for their Zn^{2+}-bound complexes, the ZP probes are well suited for biological applications.

Table 1. Spectroscopic and Thermodynamic Data for ZP Chemosensors **1–7**

	Excitation		Emission			
	(λ/nm, ϵ/ $\times$ 10^4 $M^{-1}cm^{-1}$)		(λ/nm, ϕ)[a]		pK_a[b]	K_d/nM
	Unbound	Zn^{2+} Bound	Unbound	Zn^{2+} Bound		
ZP1 (**1**)	515, 7.9	507, 8.4	531, 0.38	527, 0.87	8.4	0.7
ZP2 (**2**)	498, 4.4	490, 5.3	522, 0.25	517, 0.92	9.4	0.5
ZP3 (**3**)	502, 7.5	492, 8.5	521, 0.15	516, 0.92	6.8	0.7
ZPF1 (**4**)	533, 9.9	525, 12.0	547, 0.11	544, 0.55	6.9	0.9
ZPCl1 (**5**)	534, 9.7	527, 12.0	550, 0.22	549, 0.50	7.0	1.1
ZPBr1 (**6**)	534, 4.5	528, 8.6	549, 0.25	547, 0.36	7.3	0.9
ZPF3 (**7**)	520, 8.7	510, 9.3	537, 0.14	533, 0.60	6.7	0.8

All spectroscopic measurements were performed using 50 mM PIPES (piperazine-*N,N′*-bis(2-ethanesulfonic acid)), 100 mM KCl buffer (pH 7).
[a] Reported quantum yields are based on fluorescein, $\phi = 0.95$ in 0.1 N NaOH.
[b] Represents the pK_a value of the tertiary nitrogen responsible for PET switching in the Zn^{2+}-responsive ZP probes.

Electronegative substituents appreciably influence the electronic excitation and emission profiles of the DPA-derivatized fluoresceins. Bottom ring halogenation results in 20 nm red shifts for both excitation and emission maxima compared to fluoresceins derived from unsubstituted phthalic anhydride. In addition, top ring chlorinations at the 2′ and 7′ positions induce red shifts of 10–15 nm for excitation and emission maxima relative to unsubstituted and fluorinated dyes. By varying the combinations of electronegative substitution patterns on a homologous fluorescein skeleton, the ZP family affords a tunable optical range approaching 40 nm.

The effects of electronegative substitution on fluorescence properties of the ZP probes **3–7** are striking. For example, Figure 2 compares the pH-dependent emission profiles for ZP1, ZP2, and ZP3. The difluoro derivative ZP3 exhibits markedly reduced fluorescence within the physiological pH range relative to dichloro ZP1 and unsubstituted ZP2. The high plateau regions of the pH-dependent fluorescence response curves for ZP1, ZP2, and ZP3 correspond to a state of the chemosensor where the tertiary nitrogen atoms are protonated. The assignment of these protonation events and the corresponding pK_a values to the tertiary DPA nitrogen atoms rather than the phenolic hydroxyl group of fluorescein is based on the fact that protonation of the amines relieves PET within the fluorescein chromophore and leads to an increase in fluorescence [37], whereas protonation of the phenolic group results in a fluorescence decrease for the fluorescein backbone [19]. The observed fluorescence quantum yields for the unbound chemosensors generally track their PET nitrogen pK_a values. Plots of integrated emission intensity versus pH reveal that the tertiary nitrogen of ZP3 responsible for PET signaling has a pK_a of 6.8, resulting in a fluorescence quantum yield of 0.15 for the free probe. These experimental values are notably reduced compared to ZP1 (pK_a = 8.4, $\phi = 0.38$) and ZP2 (pK_a = 9.4, $\phi = 0.25$). Moreover, the fluorinated dyes ZPF1 (pK_a = 6.9, $\phi = 0.11$) and ZPF3 (pK_a = 6.7, $\phi = 0.14$) also display pK_a values below physiological pH with attendant low quantum yields.

Upon addition of up to 1 equiv. of Zn^{2+}, the fluorescence intensities of the ZP chemosensors increase, with concomitant blue shifts for both excitation (6–10 nm) and emission (1–5 nm) maxima (Table 1). For example, in the absence of Zn^{2+}, ZP3 has an excitation maximum of 498 nm and an emission maximum of 521 nm. After the addition of Zn^{2+}, these maxima shift to 490 nm and 516 nm, respectively. The observed hypsochromic shifts in the excitation maxima upon metal ion binding are indicative of coordination by the fluorescein phenol donor atom, which perturbs the electronic structure of fluorophore π system.

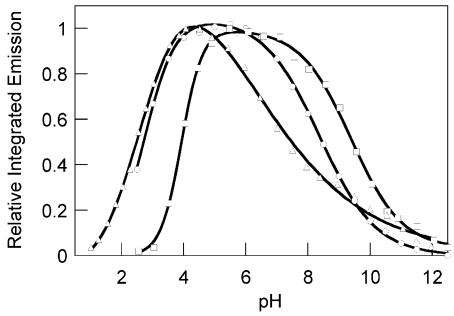

Figure 2. Graph of the Normalized Integrated Emission Intensities versus pH Values for ZP Probes

ZP1, circles; ZP2, squares; and ZP3, triangles. Titrations were performed in 100 mM KCl.

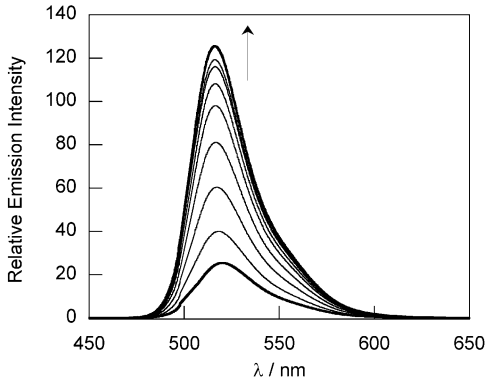

Figure 3. Fluorescence Spectroscopic Response of 0.5 μM ZP3 to Buffered Zn^{2+} Solutions

Spectra were acquired in 50 mM PIPES, 100 mM KCl (pH 7). Excitation was provided at 502 nm. The spectra shown are for free Zn^{2+} buffered at 0, 0.17, 0.42, 0.79, 1.3, 2.1, 3.4, 5.6, and 10.2 nM, respectively.

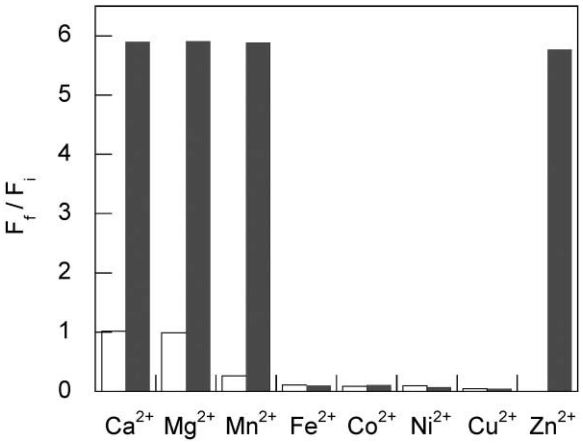

Figure 4. Fluorescence Spectroscopic Responses of ZP3 to Various Metal Ions

Bars represent the final integrated fluorescence response (F_f) over the initial integrated emission (F_i). Initial spectra were acquired in 50 mM PIPES, 100 mM KCl (pH 7). White bars represent the addition of an excess of the appropriate metal ion (2 mM for Ca^{2+} and Mg^{2+}, 50 μM for all other metal ions) to a 1 μM solution of ZP3. Gray bars represent the subsequent addition of 50 μM Zn^{2+} to the solution. Excitation was provided at 502 nm, and the emission was integrated between 505 and 650 nm.

ZP3 displays the highest dynamic range of the dyes surveyed, exhibiting over a 6-fold increase in quantum efficiency upon binding Zn^{2+} ($\phi = 0.15$ to 0.92; Figure 3), with the highest brightness reported yet for a Zn^{2+}-specific fluorescent chemosensor ($\epsilon \times \phi = 7.8 \times 10^4$ $M^{-1}cm^{-1}$). These values represent a 3-fold improvement in fluorescence quantum yield response to Zn^{2+} compared to the parent compound ZP1. It is interesting that the observed fluorescence turn-on responses depend on the choice of top and bottom ring substitutions. ZP probes **1–3** derived from unsubstituted bottom ring fluorophores are characterized by high quantum efficiencies for their Zn^{2+}-coordinated forms ($\phi \sim 0.9$). In contrast, ZP dyes **4–7** bearing bottom ring halogen groups display lower fluorescence enhancements for their Zn^{2+}-bound complexes ($\phi < 0.6$). Taken together, our results show that the simple substitution of two top ring chlorine atoms for fluorine atoms affords an effective way to control fluorophore pK_a and proton-interfering fluorescence of the apo probe while maintaining a near unity quantum efficiency upon analyte recognition.

The fluorescence responses of the electronegatively substituted ZP probes are Zn^{2+} selective. Figure 4 depicts the fluorescence responses of ZP3 to the presence of various divalent metal ions. The emission profiles of the free or Zn^{2+}-bound ZP fluorophores remain unchanged in the presence of 2 mM Ca^{2+} or Mg^{2+}, indicating excellent selectivities for Zn^{2+} over these biologically relevant alkaline earth cations. Other first-row transition metal ions including Cu^{2+}, Ni^{2+}, Co^{2+}, Fe^{2+}, and Mn^{2+} quench the fluorescence of the ZP dyes. The sample containing Mn^{2+} affords a positive fluorescence response upon the subsequent addition of Zn^{2+}.

The binding affinities for the electronegatively substituted ZP dyes were characterized by using the standard dual-metal single-ligand buffer system [37]. Varying the total Zn^{2+} concentrations between 0 and 1 mM in the presence of constant concentrations of Ca^{2+} (2 mM) and EDTA (1 mM) delivers buffered free Zn^{2+} between 0 and 25 nM. Titrations were performed in triplicate using different preparations of Ca^{2+}/Zn^{2+}/EDTA buffers. The Zn^{2+} affinities for the DPA-functionalized ZP probes are largely unaffected by fluorophore substitution. Apparent K_d values for the fluorescence-responsive 1:1 Zn^{2+}-ZP complexes range from 0.5 to 1.1 nM (Table 1), consistent with ability of the flanking picolyl groups to chelate the Zn^{2+} analyte tightly. The binding of a second Zn^{2+} atom to the ZP probes, occurring in the 9 to 85 μM range, does not change the fluorescence of the platform [37].

Fluorescence Detection of Zn^{2+} in Live Hippocampal Neurons and Slices

With a firm understanding of the spectroscopic properties and Zn^{2+}-specific fluorescence responses of the electronegatively substituted ZP chemosensors in hand, we sought to apply these new probes for the optical detection of ionic Zn^{2+} in biological samples. Imaging studies in live hippocampal neurons and slices were performed with the ZP3 fluorophore, owing to its superior brightness and dynamic range. Initial experiments with ZP3 demonstrate the ability of the electronegatively substituted ZP dyes to respond reversibly to changes in $[Zn^{2+}]$ within primary neurons in culture (Figure 5A). Incubation of cultured embryonic hippocampal neurons with 10 μM ZP3 for 20 min at 37°C results in faint punctate intracellular staining, as determined from scanning confocal fluorescence microscopy measurements on live samples. Prompt increases in cytosolic fluorescence are observed upon the addition of physiologically relevant concentrations of exogenous Zn^{2+} (50 μM) as the pyrithione (2-mercaptopyridine *N*-oxide) complex. The fluorescence enhancements are reversed by treatment with the membrane-permeable metal ion chelator TPEN [*N,N,N′,N′*-tetra(2-picolyl)ethylenediamine, 50 μM]. The residual fluorescence following TPEN treatment may arise from protonated or compartmentalized forms of apo-ZP3. The foregoing experiments establish that the ZP probes can passively enter into live neurons and monitor changes in the intracellular concentrations of Zn^{2+} reversibly.

We next sought to demonstrate the ability of the ZP dyes to image *endogenous* stores of neuronal Zn^{2+} and to apply these chemosensors for use in intact tissue samples. To this end, acute hippocampal slices from adult rats were incubated with 10 μM ZP3 for 20 min at 37°C. Figure 5B displays the confocal fluorescence image of an entire slice section of a rat hippocampus showing all of the different zinc-containing cytoarchitectonic regions. Intense fluorescence staining is detected in the hilus of the dentate gyrus and the stratum lucidum of the CA3 region. The distribution of fluorescence is consistent with other staining methods [4, 41] and indicates the large amounts of chelatable, vesicular Zn^{2+} concentrated in the mossy fiber projections connecting the fields of dentate gyrus and CA3 neurons. The vivid fluorescence derived from ionic Zn^{2+} staining is reversed by subsequent incubation of the hippocampal slices with the chelator TPEN (50 μM).

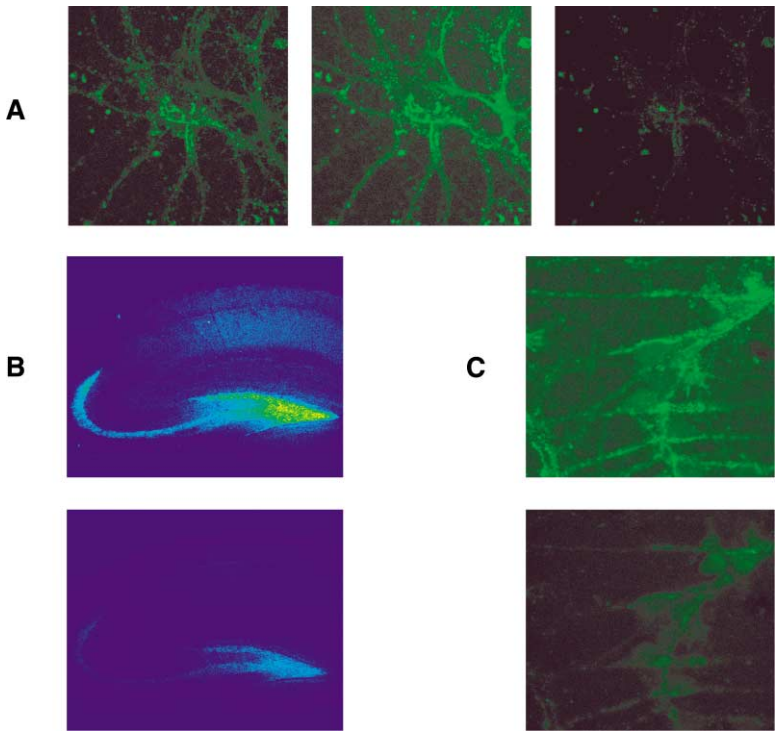

Figure 5. Fluorescence Detection of Labile Zinc Pools in Live Hippocampal Neurons and Slices

(A) Confocal fluorescence images of live hippocampal neurons labeled with ZP3. Incubation of neurons with 10 μM ZP3 for 20 min at 37°C (left), ZP3-stained neurons loaded with 50 μM $Zn(pyrithione)_2$ for 6 min (middle), and reversal of the bright cytosolic staining with 50 μM TPEN (right). Confocal images were taken from a middle optical section (vertical dimension) of the neuron.

(B) Confocal fluorescence images of an acute hippocampal slice stained with ZP3. Incubation of a slice with 10 μM ZP3 for 20 min at 37°C (top) and depletion of Zn^{2+}-derived staining by treatment with 50 μM TPEN for 20 min at 37°C (bottom).

(C) Confocal fluorescence images of live dentate gyrus neurons labeled with ZP3. Incubation of neurons with 10 μM ZP3 for 20 min at 37°C (top) and diminution of Zn^{2+}-induced fluorescence by the addition of 50 μM TPEN (bottom).

Finally, we were interested in expanding the utility of the ZP chemosensors by performing imaging studies to visualize endogenous pools of Zn^{2+} with subcellular resolution (Figure 5C). Accordingly, neuronal cultures isolated from the hippocampal dentate gyrus tissues of 4- and 5-day-old rats were loaded with ZP3 using standard conditions (10 μM probe, 20 min, 37°C). Confocal microscopy measurements reveal that these neurons show bright fluorescence labeling of intracellular Zn^{2+} and that the observed optical stainings appear in localized regions of the cell. As anticipated, the fluorescence signals produced by ionic Zn^{2+} staining are depleted by the addition of TPEN (50 μM).

Significance

We have presented electronegative substitution as a general strategy for designing effective PET chemosensors for biological imaging applications. This approach has been utilized to develop improved fluorescent probes for neuronal Zn^{2+} by controlling proton-interfering fluorescence of the apo sensors under physiological conditions. In particular, we have exploited the synthetic versatility of the fluorescein scaffold to access new Zn^{2+}-specific fluorophores with a variety of electronegative substitution patterns. The electronegatively substituted ZP probes display a tunable range of optical excitation and detection profiles in the visible wavelength regime, tunable pK_a values below physiological pH, and turn-on responses to Zn^{2+} with high brightness, metal ion selectivity, and reversibility. The fluorinated ZP3 chemosensor exhibits a 3-fold enhancement in dynamic range over the first-generation dyes ZP1 and ZP2. We have demonstrated the value of these improved detection platforms for biological applications. ZP3 has been utilized for imaging endogenous pools of ionic Zn^{2+} in live hippocampal neurons and slices. Taken together, our findings reveal that careful control of fluorophore pK_a is critical to minimizing proton-interfering fluorescence from apo probes and that electronegative substitution offers an effective general strategy for tuning PET chemosensors for cellular studies. We are now poised to apply these and related small molecule probes to interrogate the metalloneurochemistry of Zn^{2+}, with particular interest in the real-time imaging of ionic Zn^{2+} translocation in living neurons and brain slices.

Experimental Procedures

Synthetic Materials and Methods

Silica gel 60 (70–230 mesh, Merck) was used for column chromatography. Analytical thin layer chromatography was performed using Merck 60 F254 silica gel (precoated sheets, 0.25 mm thick). Solvents for synthesis were of reagent grade or better and were dried according to standard methods [42]. Literature procedures were used for the synthesis of 4-fluororesorcinol [43], 2′,7′-difluorofluorescein [44], 3,4,5,6-tetrafluoro-2′,7′-dichlorofluorescein [45], and 2′,3,4,5,6,7′-hexafluorofluorescein [44]. The compounds 2′,3,4,5,6,7′-hexafluorofluorescein and 3,4,5,6-tetrabromo-2′,7′-dichlorofluorescein were synthesized by using the method described for 3,4,5,6-tetrafluoro-2′,7′-dichlorofluorescein. ZP1 and ZP2 were available from previous studies [37]. All other chemicals were used as received.

^1H, ^{13}C, and ^{19}F NMR spectra were collected in $CDCl_3$ or d_4-methanol (Cambridge Isotope Laboratories) at the MIT Department of Chemistry Instrumentation Facility (DCIF) using either an Inova 500 or a Mercury 300 spectrometer at 25°C. All chemical shifts are reported using the standard δ notation in parts per million; positive chemical shifts are to higher frequency from the given reference. $CFCl_3$ was employed as an external standard for ^{19}F NMR measurements. Infrared spectra were acquired as KBr pellets or thin films on NaCl plates using a ThermoNicolet Avatar 360 FTIR instrument. High-resolution mass spectral analyses were carried out at the MIT DCIF.

Synthesis of Probes

9′-(2-Carboxyphenyl)-2′,7′-Difluoro-4′,5′-Bis-[Bis (2-Pyridylmethyl)-Aminomethyl]-6′-Hydroxy-3′-Xanthanone (ZP3, 3)

Di-(2-picolyl)amine (152 mg, 0.76 mmol) and paraformaldehyde (20 mg, 0.69 mmol) were combined in 4 ml of dry acetonitrile and refluxed for 1 hr under argon. A slurry of 2′,7′-difluorofluorescein (90 mg, 0.24 mmol) in 5 ml of acetonitrile/water (1:1) was added, and the resulting solution was refluxed for 24 hr under argon. The reaction was cooled to room temperature, and the precipitate was isolated by filtration. Recrystallization of the solid from ethanol afforded pure chemosensor **3** as a pale peach powder (170 mg, 88% yield). ^{1}H NMR ($CDCl_3$, 500 MHz): δ 8.59 (4 H, d, J = 4.0 Hz), 8.02 (1 H, d, J = 7.5 Hz), 7.64–7.71 (6 H, m), 7.38 (d, 4 H, J = 7.5 Hz), 7.21 (5 H, t, J = 7.5 Hz), 6.37 (2 H, d, J = 11.0 Hz), 4.20 (4 H, s), 3.98–4.06 (8 H, m). ^{13}C NMR ($CDCl_3$, 125 MHz): δ 169.02, 158.05, 151.96, 149.66, 149.05, 148.95, 148.87, 147.74, 146.45, 137.32, 135.22, 130.21, 127.40, 125.43, 124.28, 123.41, 122.64, 113.25, 108.19, 84.16, 59.31, 49.33. ^{19}F NMR ($CDCl_3$, 300 MHz): δ 36.44 (2F, s). FTIR (KBr, cm^{-1}): 3460, 3021, 2939, 2840, 2803, 1749, 1641, 1593, 1570, 1492, 1477, 1436, 1377, 1298, 1290, 1251, 1203, 1104, 1035, 997, 987, 974, 955, 894, 883, 865, 764, 754, 714, 613. HRMS (ESI) calculated for $[M+H]^+$ 791.2788, found 791.2763.

9′-(3,4,5,6-Tetrafluoro-2-Carboxyphenyl)-2′,7′-Dichloro-4′,5′-Bis-[Bis(2-Pyridylmethyl)-Aminomethyl]-6′-Hydroxy-3′-Xanthanone (ZPF1, 4)

Di-(2-picolyl)amine (400 mg, 2.01 mmol) and paraformaldehyde (60 mg, 2.07 mmol) were combined in 7 ml of dry acetonitrile and refluxed for 40 min under argon. A slurry of 3,4,5,6-tetrafluoro-2′,7′-dichlorofluorescein (300 mg, 0.63 mmol) in 10 ml of acetonitrile/water (1:1) was added, and the resulting solution was refluxed for 24 hr under argon. The reaction was cooled to room temperature, and the precipitate was isolated by filtration. Recrystallization of the solid from ethanol delivered pure fluorophore **4** as a faint salmon-colored powder (460 mg, 81% yield). ^{1}H NMR ($CDCl_3$, 300 MHz): δ 8.59 (4 H, d, J = 4.8 Hz), 7.67 (4 H, td, J = 1.5, 7.5 Hz), 7.35 (4 H, d, J = 7.5 Hz), 7.20 (4 H, t, J = 5.1 Hz), 6.80 (2 H, s), 4.17 (4 H, s), 4.01 (8 H, s). ^{13}C NMR ($CDCl_3$, 125 MHz): δ 162.74, 157.62, 156.81, 148.82, 148.27, 147.73, 146.83, 146.74, 145.12, 144.74, 143.34, 142.98, 142.55, 141.28, 140.54, 137.38, 134.06, 126.56, 123.41, 123.16, 122.71, 118.25, 112.34, 110.41, 107.11, 59.20, 49.21. ^{19}F NMR ($CDCl_3$, 300 MHz): δ 38.14 (1 F, m), 34.37 (1 F, s), 33.99 (1 F, t, J = 19.2 Hz), 26.33 (1 F, t, J = 22.5 Hz). FTIR (KBr, cm^{-1}): 3426, 3013, 2923, 2858, 2613, 1779, 1624, 1591, 1516, 1501, 1473, 1435, 1287, 1216, 1194, 1114, 1023, 764. HRMS (ESI) calculated for $[M+H]^+$ 895.1826, found 895.1831.

9′-(3,4,5,6-Tetrachloro-2-Carboxyphenyl)-2′,7′-Dichloro-4′,5′-Bis-[Bis(2-Pyridylmethyl)-Aminomethyl]-6′-Hydroxy-3′-Xanthanone (ZPCl1, 5)

Di-(2-picolyl)amine (4.00 g, 20.1 mmol) and paraformaldehyde (602 mg, 20.8 mmol) were combined in 60 ml of dry acetonitrile and refluxed for 30 min under argon. A slurry of 2′,3,4,5,6,7′-hexachlorofluorescein (3.42 g, 6.35 mmol) in 90 ml of acetonitrile/water (1:1) was added, and the resulting solution was refluxed for 24 hr under argon. The reaction was cooled to room temperature, and the precipitate was isolated by filtration and washed with water (3 × 30 ml). Recrystallization of the solid from ethanol furnished pure fluorescein **5** as a pink powder (5.50 g, 90% yield). ^{1}H NMR ($CDCl_3$, 500 MHz): δ 8.60 (4 H, d, J = 6.0 Hz), 7.66 (4 H, td, J = 1.5, 7.5 Hz), 7.34 (4 H, d, J = 7.5 Hz), 7.20 (4 H, t, J = 5.0 Hz), 6.76 (2 H, s), 4.17 (4 H, s), 3.95-4.02 (8 H, m). ^{13}C NMR ($CDCl_3$, 125 MHz): δ 164.05, 157.71, 156.53, 149.09, 148.87, 148.71, 140.88, 137.41, 136.66, 131.29, 128.38, 126.75, 123.42, 122.87, 122.72, 118.13, 112.06, 106.46, 81.29, 59.14, 49.17. FTIR (KBr, cm^{-1}): 3431, 3011, 2921, 1784, 1626, 1590, 1570, 1470, 1434, 1381, 1322, 1283, 1214, 1145, 1020, 929, 912, 760, 735. HRMS (ESI) calculated for $[M+H]^+$ 959.0638, found 959.0672.

9′-(3,4,5,6-Tetrabromo-2-Carboxyphenyl)-2′,7′-Dichloro-4′,5′-Bis-[Bis(2-Pyridylmethyl)-Aminomethyl]-6′-Hydroxy-3′-Xanthanone (ZPBr1, 6)

Di-(2-picolyl)amine (2.00 g, 10.0 mmol) and paraformaldehyde (301 mg, 10.4 mmol) were combined in 30 ml of dry acetonitrile and refluxed for 45 min under argon. A slurry of 3,4,5,6-tetrabromo-2′,7′-dichlorofluorescein (2.27 g, 3.17 mmol) in 30 ml of acetonitrile/water (1:1) was added, and the resulting solution was refluxed for 24 hr under argon. The reaction was cooled to room temperature, and the precipitate was isolated by filtration and washed with water (3 × 35 ml). Recrystallization of the solid from ethanol gave pure product **6** as a pale pink powder (3.18 g, 88% yield). ^{1}H NMR ($CDCl_3$, 500 MHz): δ 8.60 (4 H, d, J = 6.0 Hz), 7.66 (4 H, td, J = 2.0, 7.5 Hz), 7.33 (4 H, d, J = 8.0 Hz), 7.19 (4 H, t, J = 5.0 Hz), 6.72 (2 H, s), 4.16 (4 H, s), 3.94-4.01 (8 H, m). ^{13}C NMR ($CDCl_3$, 125 MHz): δ 164.31, 157.73, 156.48, 151.89, 148.99, 148.89, 138.28, 137.41, 133.65, 126.86, 125.89, 123.54, 123.39, 122.71, 121.90, 118.11, 111.95, 106.45, 82.02, 59.11, 49.12. FTIR (KBr, cm^{-1}): 3436, 3009, 2920, 1779, 1625, 1589, 1570, 1473, 1433, 1399, 1358, 1282, 1258, 1202, 1130, 1047, 995, 951, 909, 753, 708, 675, 639. HRMS (ESI) calculated for $[M+H]^+$ 1134.8618, found 1134.8656.

9′-(3,4,5,6-Tetrafluoro-2-Carboxyphenyl)-2′,7′-Difluoro-4′,5′-Bis-[Bis(2-Pyridylmethyl)-Aminomethyl]-6′-Hydroxy-3′-Xanthanone (ZPF3, 7)

Di-(2-picolyl)amine (96 mg, 0.48 mmol) and paraformaldehyde (15 mg, 0.52 mmol) were combined in 3 ml of dry acetonitrile and refluxed for 40 min under argon. A slurry of 2′,3,4,5,6,7′-hexafluorofluorescein (68 mg, 0.15 mmol) in 5 ml of acetonitrile/water (1:1) was added, and the resulting solution was refluxed for 24 hr under argon. The reaction was cooled to room temperature, and the precipitate was isolated by filtration and washed with water (3 × 10 ml). Recrystallization of the solid from ethanol supplied pure dye **7** as an orange powder (106 mg, 80% yield). ^{1}H NMR ($CDCl_3$, 500 MHz): δ 8.58 (4 H, d, J = 6.0 Hz), 7.65 (4 H, td, J = 1.5, 7.8 Hz), 7.34 (4 H, d, J = 7.5 Hz), 7.19 (4 H, t, J = 5.0 Hz), 6.53 (2 H, d, J = 10.0 Hz), 4.16 (4 H, s), 3.96-4.03 (8 H, m). ^{13}C NMR ($CDCl_3$, 125 MHz): δ 157.90, 149.49, 148.71, 137.34, 136.87, 123.35, 122.64, 113.63, 111.97, 59.24, 53.92, 53.23, 50.86, 49.04, 29.88. ^{19}F NMR ($CDCl_3$, 300 MHz): δ 43.70 (2 F, s), 36.42 (1 F, s), 35.06 (1 F, s), 26.33 (1 F, s), 19.61 (1 F, s). FTIR (KBr, cm^{-1}): 3400, 3052, 3011, 2925, 2854, 1773, 1593, 1571, 1478, 1437, 1376, 1292, 1207, 1169, 1044, 996, 763, 628. HRMS (ESI) calculated for $[M+H]^+$ 863.2411, found 863.2398.

Spectroscopic Materials and Methods

Ultrol grade PIPES (piperazine-*N,N′*-bis(2-ethanesulfonic acid)), Calbiochem), KCl (Alfa, Puratronic grade, 99.997%), and $ZnCl_2$ (Aldrich, 99.999%) were used as received. Millipore water was used for all aqueous solutions, and the solutions were filtered through 0.2 μm cellulose filters prior to use. With the exception of the pK_a experiments, all spectroscopic measurements were performed under simulated physiological conditions using buffer solutions containing 50 mM PIPES and 100 mM KCl adjusted to pH 7. A glass electrode (Orion), calibrated prior to each use, was used to determine solution pH. Solutions of Zn^{2+} were prepared from 100 mM stock solutions of $ZnCl_2$ in water.

Absorption spectra were obtained using either a Cary 1E scanning spectrophotometer or Hewlett-Packard 8453A diode array spectrophotometer. A circulating water bath was used during all experiments to regulate the temperature at 25°C. Samples were contained in 1 cm path length quartz cuvettes (3.5 ml volume, Starna). Fluorescence spectra were recorded using a Hitachi F-3010 spectrofluorimeter. Excitation was provided by a 150 W Xe lamp (Ushio Inc.) operating at a current of 5 A. A rhodamine quantum counter was used to normalize the spectra for excitation intensity, and manufacturer-supplied correction curves were used to normalize the emission spectra. Manufacturer-supplied photomultiplier curves were used to correct for emission intensity. A circulating water bath was used during all experiments to regulate the temperature at 25°C. All spectra were obtained using 3 nm slit widths, and samples were contained in 1 cm × 1 cm quartz cuvettes (3.5 ml volume, Starna). The experiments for measuring pH-dependent fluorescence profiles, quantum yields, apparent dissociation constants (K_d), and metal ion selectivities were performed using standard protocols [37, 38]. Quantum yields were determined by reference to fluorescein in 0.1 N NaOH (ϕ = 0.95) [46].

Preparation and Staining of Hippocampal Primary Cultures

Hippocampal primary cultures were prepared from embryonic day 19 (E19) Sprague-Dawley rat embryos according to a previously reported protocol [47]. Medium density cultures (150 cells/mm^2) were plated on live imaging dishes (MatTek Corporation, Ashland,

MA). The glass bottoms of the dishes were coated with poly-D-lysine (30 μg/ml) and laminin (2.5 μg/ml). Neuronal cultures were grown in Neurobasal media (Invitrogen, Carlsbad, CA) supplemented with B27 (Invitrogen), glutamine (0.5 mM), and glutamate (12.5 μM). After 18 days in culture, cells were stained by bath application of ZP3 (10 μM) to the media for 20 min at 37°C under 5% CO_2. Cells were then washed once with media before imaging.

Preparation and Staining of Dentate Gyrus Cultures

Primary cultures of dentate gyrus (DG) cells were obtained by modification of literature procedures [48, 49]. Dentate gyrus regions were dissected from the hippocampi of 4-day-old Sprague-Dawley rat pups. Cells were plated on 24 mm glass coverslips (250 cells/mm^2) coated with poly-L-lysine (50 μg/ml). Cultures were maintained for the first 24 hr in Dulbecco's modified Eagle's medium (DMEM, Invitrogen) supplemented with 10% fetal calf serum (FCS, Invitrogen), glutamine (2 mM), and penicillin-streptomycin mix (50 μg/ml). Subsequently, cultures were kept in the following media: Neurobasal medium (Invitrogen, Carlsbad, CA) supplemented with B27 (Invitrogen), glutamine (2 mM), potassium chloride (20 mM), and penicillin-streptomycin mix (50 μg/ml). After 7 days in culture, cells were stained by bath application of ZP3 (10 μM) to the media for 20 min at 37°C under 5% CO_2. Cells were then washed once with media before imaging.

Preparation and Staining of Acute Hippocampal Slices

The whole brains of 90-day-old adult Sprague-Dawley rats were removed. The hippocampi were dissected, cut into 0.5–1.0 mm-thick slices, and washed twice with Zn^{2+}-free Krebs ringer buffer; this medium was prepared according to a published method [50]. Slices were incubated with ZP3 (10 μM) for 20 min at 37°C under 5% CO_2. Slices were then washed twice with Zn^{2+}-free Krebs ringer buffer and transferred to glass-bottomed imaging dishes for fluorescence microscopy.

Fluorescence Imaging Experiments

Confocal fluorescence imaging experiments were performed with a Zeiss LSM510 laser scanning microscopy system having an Axiovert 200M inverted fluorescence microscope. The microscope was equipped with an argon ion laser (488 nm excitation), objective lenses (40×, embryonic hippocampal neurons and dentate gyrus neurons, 4× hippocampal slices), and a 505 nm long pass emission filter. During imaging measurements, cell and slice samples were kept on the microscope stage in a CTI-3700 incubator at 37°C under 5% CO_2. Appropriate additions of Zn^{2+} as the pyrithione complex (2-mercaptopyridine *N*-oxide) and/or TPEN [*N,N,N′,N′*-tetra(2-picolyl)ethylenediamine] to cell and slice samples were performed directly on the microscope stage by bath application to the media.

Acknowledgments

This work was supported by a grant to S.J.L. from the National Institute of General Medical Sciences (GM 65519). C.J.C. acknowledges the Jane Coffin Childs Foundation for a postdoctoral fellowship. E.M.N. thanks the U.S. Department of Defense for a National Defense Science and Engineering Graduate Fellowship. M.S. is an Investigator at the Howard Hughes Medical Institute. The MIT Department of Chemistry Instrument Facility is funded through the National Science Foundation (CHE-9808061, CHE-9808063, and DBI-9729592).

Received: October 9, 2003
Revised: November 15, 2003
Accepted: November 17, 2003
Published: February 20, 2004

References

1. Vallee, B.L., and Falchuk, K.H. (1993). The biochemical basis of zinc physiology. Physiol. Rev. *73*, 79–118.
2. Atwood, C.S., Huang, X., Moir, R.D., Tanzi, R.E., and Bush, A.I. (1999). Role of free radicals and metal ions in the pathogenesis of Alzheimer's disease. Met. Ions Biol. Syst. *36*, 309–364.
3. Lippard, S.J., and Berg, J.M. (1994). Principles of Bioinorganic Chemistry, First Edition (Mill Valley, CA: University Science Books).
4. Frederickson, C.J. (1989). Neurobiology of zinc and zinc-containing neurons. Int. Rev. Neurobiol. *31*, 145–238.
5. Takeda, A. (2001). Zinc homeostasis and functions of zinc in the brain. Biometals *14*, 343–351.
6. Frederickson, C.J., and Bush, A.I. (2001). Synaptically released zinc: Physiological functions and pathological effects. Biometals *14*, 353–366.
7. Vogt, K., Mellor, J., Tong, G., and Nicoll, R. (2000). The actions of synaptically released zinc at hippocampal mossy fiber synapses. Neuron *26*, 187–196.
8. Ueno, S., Tsukamoto, M., Hirano, T., Kikuchi, K., Yamada, M.K., Nishiyama, N., Nagano, T., Matsuki, N., and Ikegaya, Y. (2001). Mossy fiber Zn^{2+} spillover modulates heterosynaptic N-methyl-D-aspartate receptor activity in hippocamapal CA3 circuits. J. Cell Biol. *158*, 215–220.
9. Li, Y., Hough, C.J., Frederickson, C.J., and Sarvey, J.M. (2001). Induction of mossy fiber CA3 long-term potentiation requires translocation of synaptically released Zn^{2+}. J. Neurosci. *21*, 8015–8025.
10. Choi, D.W., and Koh, J.Y. (1998). Zinc and brain injury. Annu. Rev. Neurosci. *21*, 347–375.
11. Bush, A.I. (2000). Metals and neuroscience. Curr. Opin. Chem. Biol. *4*, 184–191.
12. Bush, A.I. (2003). The metallobiology of Alzheimer's disease. Trends Neurosci. *26*, 207–214.
13. Cuajungco, M.P., and Lees, G.J. (1997). Zinc metabolism in the brain: Relevance to human neurodegenerative disorders. Neurobiol. Dis. *4*, 137–169.
14. Suh, S.W., Jensen, K.B., Jensen, M.S., Silva, D.S., Kesslak, P.J., Danscher, G., and Frederickson, C.J. (2000). Histochemically-reactive zinc in amyloid plaques, angiopathy, and degenerating neurons of Alzheimer's diseased brains. Brain Res. *852*, 274–278.
15. Rowan, M.J., Klyubin, I., Cullen, W.K., and Anwyl, R. (2003). Synaptic plasticity in animal models of early Alzheimer's disease. Philos. Trans. R Soc. Lond. B Biol. Sci. *358*, 821–828.
16. Kay, A.R. (2003). Evidence for chelatable zinc in the extracellular space of the hippocampus, but little evidence for the synaptic release of Zn. J. Neurosci. *23*, 6847–6855.
17. Burdette, S.C., and Lippard, S.J. (2003). Meeting of the minds: Metalloneurochemistry. Proc. Natl. Acad. Sci. USA *100*, 3605–3610.
18. Burdette, S.C., and Lippard, S.J. (2001). ICCC34-golden edition of coordination chemistry reviews. Coordination chemistry for the neurosciences. Coord. Chem. Rev. *216–217*, 333–361.
19. Hirano, T., Kikuchi, K., Urano, Y., and Nagano, T. (2002). Improvement and biological applications of fluorescent probes for zinc, ZnAFs. J. Am. Chem. Soc. *124*, 6555–6562.
20. Gee, K.R., Zhou, Z.L., Ton-That, D., Sensi, S.L., and Weiss, J.H. (2002). Measuring zinc in living cells. A new generation of sensitive and selective fluorescent probes. Cell Calcium *31*, 245–251.
21. Czarnik, A.W. (1994). Chemical communications in water using fluorescent chemosensors. Acc. Chem. Res. *27*, 302–308.
22. Thompson, R.B., Cramer, M.L., Bozym, R., and Fierke, C.A. (2002). Excitation ratiometric fluorescent biosensor for zinc ion at picomolar levels. J. Biomed. Opt. *7*, 555–560.
23. Godwin, H.A., and Berg, J.M. (1996). A fluorescent zinc probe based on metal-induced peptide folding. J. Am. Chem. Soc. *118*, 6514–6515.
24. Shults, M.D., Pearce, D.A., and Imperiali, B. (2003). Modular and tunable chemosensor scaffold for divalent zinc. J. Am. Chem. Soc. *125*, 10591–10597.
25. Aoki, S., Kaido, S., Fujioka, H., and Kimura, E. (2003). A new zinc(II) fluorophore 2-(9-anthrylmethylamino)ethyl-appended 1,4,7,10-tetraazacyclododecane. Inorg. Chem. *42*, 1023–1030.
26. Dai, Z., Xu, X., and Canary, J.W. (2002). Stereochemical control of Zn(II)/Cu(II) selectivity in piperidine tripod ligands. Chem. Commun., 1414–1415.
27. Jiang, P., Chen, L., Lin, J., Liu, Q., Ding, J., Gao, X., and Guo,

Z. (2002). Novel zinc fluorescent probe bearing dansyl and aminoquinoline groups. Chem. Commun., 1424–1425.
28. Kim, T.W., Park, J.-h., and Hong, J.-I. (2002). Zn^{2+} fluorescent chemosensors and the influence of their spacer length on tuning Zn^{2+} selectivity. J. Chem. Soc. Perkin *2*, 923–927.
29. Kimber, M.C., Mahadevan, I.B., Lincoln, S.F., Ward, A.D., and Tiekink, E.R.T. (2000). The synthesis and fluorescent properties of analogues of the zinc(II) specific fluorophore zinquin ester. J. Org. Chem. *65*, 8204–8209.
30. Lim, N.C., Yao, L., Freake, H.C., and Brückner, C. (2003). Synthesis of a fluorescent chemosensor suitable for the imaging of zinc(II) in live cells. Bioorg. Med. Chem. Lett. *13*, 2251–2254.
31. Nasir, M.S., Fahrni, C.J., Suhy, D.A., Kolodsick, K.J., Singer, C.P., and O'Halloran, T.V. (1999). The chemical cell biology of zinc: structure and intracellular fluorescence of a zinc-quinolinesulfonamide complex. J. Biol. Inorg. Chem. *4*, 775–783.
32. Xue, G., Bradshaw, J.S., Dalley, N.K., Savage, P.B., Izatt, R.M., Prodi, L., Montalti, M., and Zaccheroni, N. (2002). The synthesis of azacrown ethers with quinoline-based sidearms as potential zinc(II) fluorophores. Tetrahedron *58*, 4809–4815.
33. Gunnlaugsson, T., Lee, T.C., and Parkesh, R. (2003). A highly selective and sensitive fluorescent PET (photoinduced electron transfer) chemosensor for Zn(II). Org. Biomol. Chem. *1*, 3265–3267.
34. Tsien, R.Y. (1989). Fluorescent indicators of ion concentrations. Methods Cell Biol. *30*, 127–156.
35. de Silva, A.P., Gunaratne, H.Q.N., Gunnlaugsson, T., Huxley, A.J., McCoy, C.P., Rademacher, J.T., and Rice, T.E. (1997). Signaling and recognition events with fluorescent sensors and switches. Chem. Rev. *97*, 1515–1566.
36. Walkup, G.K., Burdette, S.C., Lippard, S.J., and Tsien, R.Y. (2000). A new cell-permeable fluorescent probe for Zn^{2+}. J. Am. Chem. Soc. *122*, 5644–5645.
37. Burdette, S.C., Walkup, G.K., Spingler, B., Tsien, R.Y., and Lippard, S.J. (2001). Fluorescent sensors for Zn^{2+} based on a fluorescein platform: Synthesis, properties and intracellular distribution. J. Am. Chem. Soc. *123*, 7831–7841.
38. Burdette, S.C., Frederickson, C.J., Bu, W., and Lippard, S.J. (2003). ZP4, an improved neuronal Zn^{2+} sensor of the Zinpyr family. J. Am. Chem. Soc. *125*, 1778–1787.
39. Woodroofe, C.C., and Lippard, S.J. (2003). A novel two-fluorophore approach to ratiometric sensing of Zn^{2+}. J. Am. Chem. Soc. *125*, 11458–11459.
40. Nolan, E.M., Burdette, S.C., Harvey, J.H., Hilderbrand, S.A., and Lippard, S.J. (2004). Synthesis and characterization of zinc sensors based on a monosubstituted fluorescein platform. Inorg. Chem., in press.
41. Danscher, G., Juhl, S., Stoltenberg, M., Krunderup, B., Schroder, H.D., and Andreasen, A. (1997). Autometallographic silver enhancement of zinc sulfide crystals created in cryostat sections from human brain biopsies: A new technique that makes it feasible to demonstrate zinc ions in tissue sections from biopsies and early autopsy material. J. Histochem. Cytochem. *45*, 1503–1510.
42. Pangborn, A.B., Giardello, M.A., Grubbs, R.H., Rosen, R.K., and Timmers, F.J. (1996). Safe and convenient procedure for solvent purification. Organomet. *15*, 1518–1520.
43. Yang, J.-J., Su, D., Vij, A., Hubler, T.L., Kirchmeier, R.L., and Shreeve, J.M. (1998). Synthesis of 4-fluororesorcinol and 4-trifluoromethylresorcinol. Heteroatom. Chem. *9*, 229–239.
44. Sun, W.-C., Gee, K.R., Klaubert, D.H., and Haugland, R.P. (1997). Synthesis of fluorinated fluoresceins. J. Org. Chem. *62*, 6469–6475.
45. Gee, K.R., Sun, W.-C., Klaubert, D.H., Haugland, R.P., Upson, R.H., Steinberg, T.H., and Poot, M. (1996). Novel derivatization of protein thiols with fluorinated fluoresceins. Tetrahedron Lett. *37*, 7905–7908.
46. Brannon, J.H., and Magde, D. (1978). Absolute quantum yield determination by thermal blooming. Fluorescein. J. Phys. Chem. *82*, 705–709.
47. Brewer, G.J., Torricelli, J.R., Evege, E.K., and Price, P.J. (1993). Optimized survival of hippocampal neurons in B27-supplemented Neurobasal, a new serum-free medium combination. J. Neurosci. Res. *35*, 567–576.
48. Figiel, I., and Kaczmarek, L. (1997). Cellular and molecular correlates of glutamate-evoked neuronal programmed cell death in the *in vitro* culture of rat hippocampal dentate gyrus. Neurochem. Int. *31*, 229–240.
49. Jaworski, J., Figiel, I., Proszynski, T., and Kaczmarek, L. (2000). Efficient expression of tetracycline-responsive gene following transfection of dentate gyrus neurons *in vitro*. J. Neurosci. Res. *60*, 754–760.
50. Qian, W.-J., Gee, K.R., and Kennedy, R.T. (2003). Imaging of Zn^{2+} release from pancreatic β-cells at the level of single exocytotic events. Anal. Chem. *75*, 3468–3475.